Model studies of non-linear wave propagation in liquid-filled visco-elastic tubes

Vakgroep Fundamentele Werktuigbouwkunde

Model studies of non-linear wave propagation in liquid-filled visco-elastic tubes.

A.A. v. Steenhoven en M.E.H. van Dongen.

WFW-rapport 85.003.
2-1-1985.

Technische Hogeschool Eindhoven.

Voorwoord

Dit rapport biedt een overzicht van de experimentele en analytische werkzaamheden zoals die in het afgelopen jaar door beide auteurs aan de zogenaamde klepsluitingsopstelling zijn uitgevoerd. Het is de bedoeling dit te zijner tijd tot publicatie te brengen, doch voor die tijd is behoefte aan reactie en discussie. Vandaar deze op een aantal punten, zoals o.a. doorwerking buiswand eigenschappen, nog incomplete versie.

Model studies of non-linear wave propagation in liquid-filled visco-elastic tubes

A.A. van Steenhoven and M.E.H. van Dongen.

Departments of Mechanical Engineering and Physics
Eindhoven University of Technology, The Netherlands.

Contents:

Summary

Model experiments are performed in a long thin-walled fluid-filled visco-elastic tube in which the fluid is suddenly slowed down starting from a steady flow. The resulting jump in pressure is determined as a function of initial flow velocity, position in the tube and for different wall inhomogeneities. The observed phenomena are analysed using one-dimensional models of wave propagation and separately the influence of non-linearities, fluid viscosity, visco-elastic wall properties and wave reflections are discussed.

Introduction

The study of non-linear wave propagation in liquid-filled visco-elastic tubes is often motivated by its application to the arterial blood flow. It is known from both static and dynamic measurements (Bergel 1961, Milnor 1982) that the walls of the large blood vessels exhibit non-linear elastic and viscous properties. The analysis of the resulting blood flow and pressure pulse wave forms at various locations in the arterial tree has been the subject of many investigations. Most often the approach was of a mathematical nature. Contributions have been given, among others by Euler (1775), Young (1808) and Lambossy (1950). For physiological applications the analysis of Womersley (1957) appeared to be important. He solved the linearised Navier-Stokes equations under assumption of small elastic deformations of the vessel wall. Later this analysis was extended by others to include the effects of initial stresses, perivascular tethering and visco-elastic behaviour of the arterial wall (Cox 1968). Also the influence of the non-linear convective acceleration terms of the Navier-Stokes equation and the geometric and elastic non-linear properties of the vessel wall have been investigated (Olson and Shapiro 1967, Ling and Atabek 1972). The physiological relevance of the latter analysis is that due to the strongly non-linear elastic behaviour of the vessel wall steepening of the wave front and consequently shock-like discontinuities are expected (Rudinger 1970, Pedley 1980 and Cowley 1982). A rather general but linear model of wave propagation in orthotropic tubes has recently been given by Kuiken (1984). In all these models the visco-elasticity of the vessel walls and blood has been neglected or oversimplified. However, as indicated by Anliker (1978) and analysed by Holenstein et al. (1980, 1984), the complete visco-elastic damping properties of arteries and blood cells need to be included in order to obtain accurate theoretical results valuable over large distances in the arterial tree.

Most of the previously mentioned mathematical models of arterial pulse propagation have been compared to in-vivo data, which is quite difficult in view of the many assumptions made in each model. Only little data is available from well-defined model experiments. An outline of such experiments was given by Kivity and Collins (1974) in order to determine the visco-elastic properties of large blood vessels. This method is based upon measurements of the axial distribution of either cross-sectional area or internal pressure during the passage of a "shock" wave in the vessel. Collins et al. (1976)

have applied the proposed analysis to experimentally produced pressure jumps in silastic tubes and used their observations to infer the visco-elastic properties of the tube. But, as stated by Pedley (1980), their results have to be examined with caution due to the assumed oversimplified model of the visco-elastic material properties.

Odou et al. (1979) reported about experiments in a visco-elastic rubber test section of a hydromechanical model. In this set-up waves were produced by rapid electrically driven piston motion and the change in tube diameter has been measured optically at various sites along its length during the passage of the wave front. However, only some introductory results were given.

Apart of the model studies described sofar, numerous attempts have been undertaken to investigate the properties of collapsing tubes. Extensive studies have been performed for example by Shapiro (1977) and Kamm and Shapiro (1979). In this case the cross-sectional area of the tube becomes highly non-circular and the non-linear elastic properties then completely dominate the observed phenomena. In the present study the internal pressure sufficiently exceeds the outer one to prevent the tube to collaps and hence these studies remain out of scope here. Finally, for an overview of the phenomena of wave propagation and a summary of in-vivo data, both concerning the circulatory system, we refer to Wetterer and Kenner (1968), Lighthill (1975), Pedley (1980), Milnor (1982) and Fung (1984).

In the present paper, model experiments are described of wave phenomena in a long uniform non-linear visco-elastic tube of well known material properties. The wave phenomena are analysed using one-dimensional models of wave propagation and separately the influence of non-linearities, fluid viscosity and wave reflections are discussed. Also a first but uncomplete attempt to describe the influence of the viscous wall properties is presented. The physiological relevance of this study is, apart from gaining more insight into wave propagation in the arterial system, more specifically the understanding of the phenomena that occur just after aortic valve closure. In previous studies we performed model and animal studies on the closing behaviour of this valve (van Steenhoven and van Dongen 1979, van Steenhoven et al. 1981/1982). The animal experiments confirmed the model findings of Bellhouse and Talbot (1969) that during deceleration of the liquid in the aorta the cross-sectional area of the valve orifice reduces about 75% and that only a small reversed flow is then sufficient to complete the closure. In the model studies we demonstrated that this gradual valve closure during flow

deceleration can mainly be described from the positive pressure gradient in axial direction. Furthermore, it was found that a small cavity behind the leaflets is essential for this early valve closure. Besides, in case the natural sinus cavities do not optimally fit to the valve leaflets, for example when a bioprosthesis is used, the necessary back flow to complete the closure increases considerably (van Steenhoven et al. 1982). However, the backflow to complete the closure needs to be suddenly slowed down by the closed valve, which causes a rise in the aortic pressure known as the dicrotic notch. From the tissues surrounding the valve Sauren et al (1983) demonstrated that the leaflet are much stiffer than the aortic wall. The latter on its turn differs slightly in elasticity from the sinus walls. Besides, all these tissues showed remarkable visco-elastic material properties. It is the ultimate goal of this study to determine the parameters which govern the pressure rise just after valve closure, as well as its magnitude and slope close to the valve as its propagation through the aorta. As a first step, in the present model study sudden valve closure is simulated starting from a steady initial flow and the resulting pressure rise is studied in relation to the wall material properties, the initial volume flow values, the distance to the valve and a negative or positive reflection coefficient at a distinct point (like the sinus-aorta connection) in the tube. First the experimental set-up, the wall material properties and some qualitative experimental observations are presented. Next some physical models based on one-dimensional wave propagation in elastic tubes are treated. Finally, a quantitative comparison of theoretical predictions with experimental data will take place.

Qualitative experimental observations

The experimental set-up

Basically, the realized set-up consists of a latex tube (Penrose Drain, length ≈ 0,6 m., internal diameter ≈ 1.8 10^{-2} m., wall thickness ≈ 2 10^{-4} m.) fixed between two reservoirs, see figure 1^{a}. The fluid used is water. Constant fluid velocities between 0.1 and 0.5 ms can be achieved by varying the constant pressure difference between the reservoirs. The tube is prevented to collaps through a transmural pressure of about 3 kPa adjusted by the fluid height in the reservoirs. On x = 0 the diameter of the latex tube is locally 20% reduced. From the left reservoir a metal tube (outer diameter = 8 10^{-3} m.) is aligned along the axis of the latex tube, the tip of it being located at the constriction C, see figure 1^{b}. From this tip towards the right reservoir four nylon threads (diameter = 5 10^{-5} m.) are stretched. Over this tube a washerlike occluder (outer diameter = 16 10^{-3} m., internal diameter = 6.5 10^{-3} m., specific weight = 10^{3} kg/m^{3}) can be taken along by the flow on the moment that the occluder is placed in the flow. A step-like reduction of the volume flow to zero is achieved on the moment that the occluder contacts both the constriction of the latex tube and the tip of the previously mentioned metal tube (closing time ≈ 15 10^{-3} s).

The time and place dependent variation in pressure was measured locally at the axis of the tube with a catheter-tip manometer (Millar PC 470) which is positioned through the metal tube as shown in figure 1. To determine the wave front distortion two catheter-tip manometers were used simultaneously, one close to the constriction and the other, analogously inserted at the right-hand side, at a distance of a multiple of 5 10^{-2} m. from the former. To measure the wall deflection during the pressure jump a photonic sensor (MTI KD-100) was used placed about 1 mm. above the tube itself. The value of volume flow was measured electromagnetically (Transflow 601) at the inflow side of the right reservoir. All electrical signals were recorded on an electromagnetic tape recorder (Hewlet-Packard 3968 A) and the pressure and wall deflection signals were analysed using a two-channel transient recorder (Datalog 912).

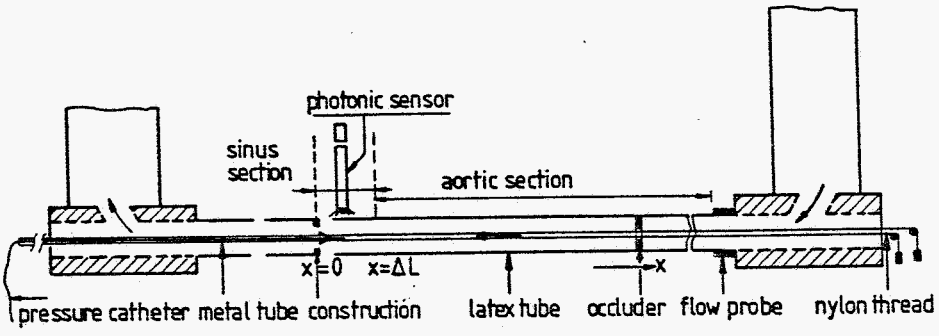

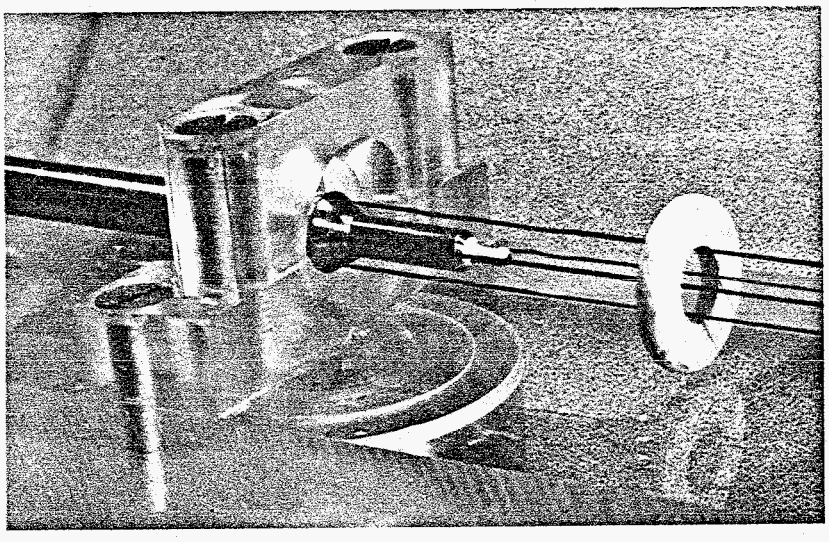

Fig. 1: a Schematic diagram of the model set-up.
b Photograph of the constriction point C when the latex tube is removed.

Tube wall properties

To determine the elastic and viscous properties of the latex tube wall, some uniaxial tensile experiments were performed. Firstly, in a tensile machine (Zwick 1434) the force-displacement relation was determined at a constant strain-rate of 0.005 s^{-1}. The specimen used in this experiment were strips approximately 4 mm in width, varying from 10 to 12 mm in length and 0.2 mm thick. A typical result is shown in figure 2. Next the properties were determined at faster strain rates and as well as the dependence of the strain value and of the strain rate were investigated. The strain variation ($\Delta\varepsilon = 0.20$) was suppressed to the specimen with the aid of an electrodynamic exciter (Ling Dynamic 2000), the resulting load was measured with a piezo-electrical load cell (Kistler 9203) and the elongation with a capacitive displacement-measuring system (Boersma CVM IV). For a detailed description of the experimental procedure we refer to Sauren et al. (1983). Typical results are given in figure 3. From these figures two quantities were determined which characterise the elastic and viscous properties, being the averaged value of the slope of the upward and downward stress-strain curve and the stress difference between both curves at a strain corresponding to half the suppressed strain variation. The relation between those quantities and the values of strain and strain rate is given in figure 4. From this it is concluded that the slope decreases with increasing strain-value, which is in accordance to the stress-strain curve given in figure 2. The stress-difference between the two stress-strain curves shows hardly no influence of the strain-rate value. This indicates that the viscoelastic material properties cannot easily be described with the aid of a simple Maxwell-model. It is finally remarked that the results of the various experiments has to be compared to each other with some carefullness due to the time elapsed between the experiments. On the other hand all experiments were performed on the same tissue strip taken from the tube in which the pressure jumps were measured.

Characteristic results

A typical result of the pressure signal in a uniform tube and close to the valve is given in figure 5. As a result of valve closure the pressure rapidly increases. The rise time of the pressure is about 10 msec. and is caused by the finite closing time of the occluder. This initial fast pressure jump is followed by a much more gradual increase, probably due to the

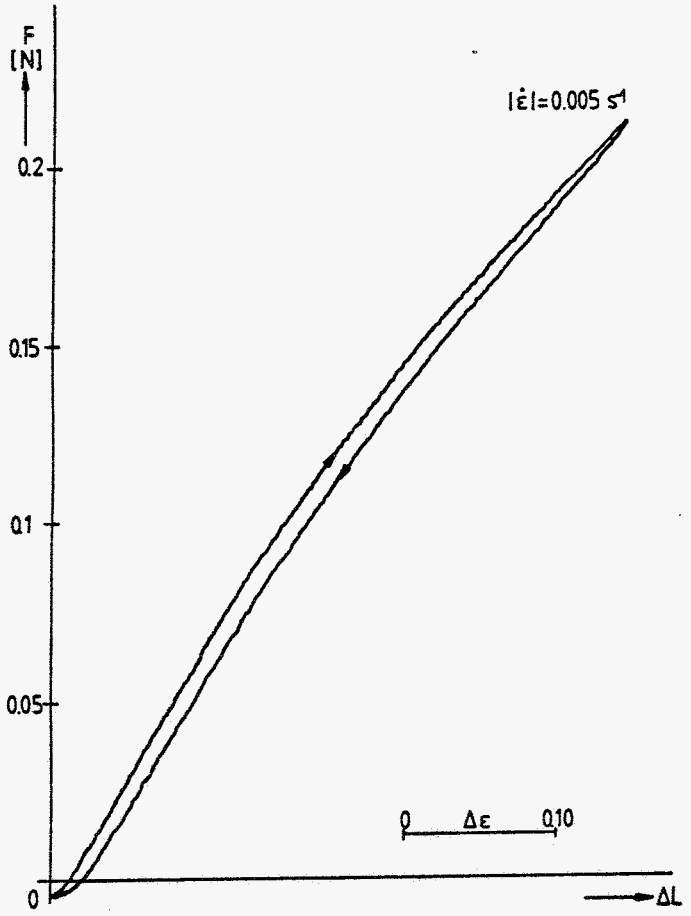

Fig. 2: Force-elongation curve of a latex specimen, at a low strain-rate (width 4.0 mm, length 10.6 mm, thickness 0.2 mm).

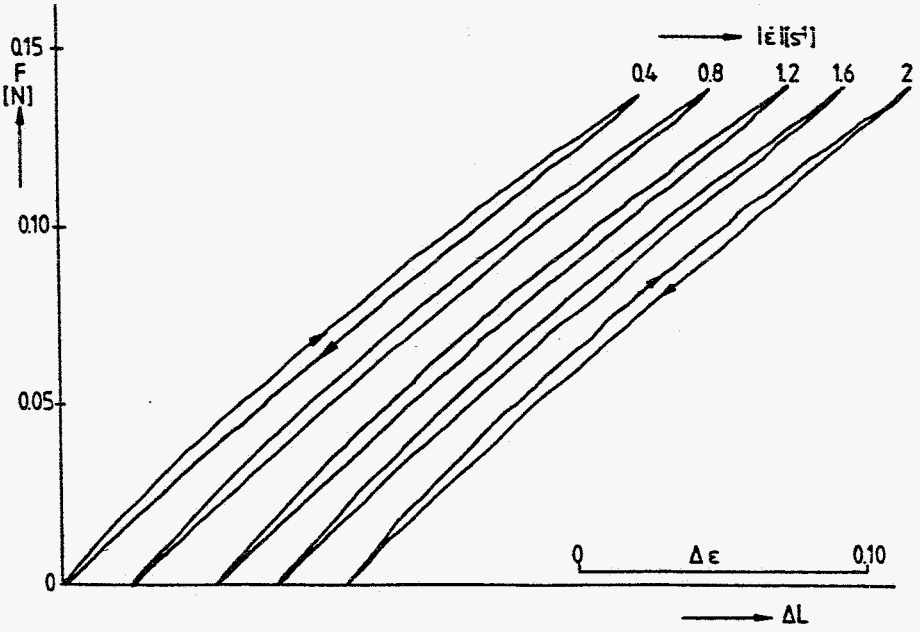

Fig. 3: Force-elongation curves of a latex specimen at higher strain-rates. (width 4.0 mm, length 11.5 mm, thickness 0.2 mm, pre-strain 0.15).

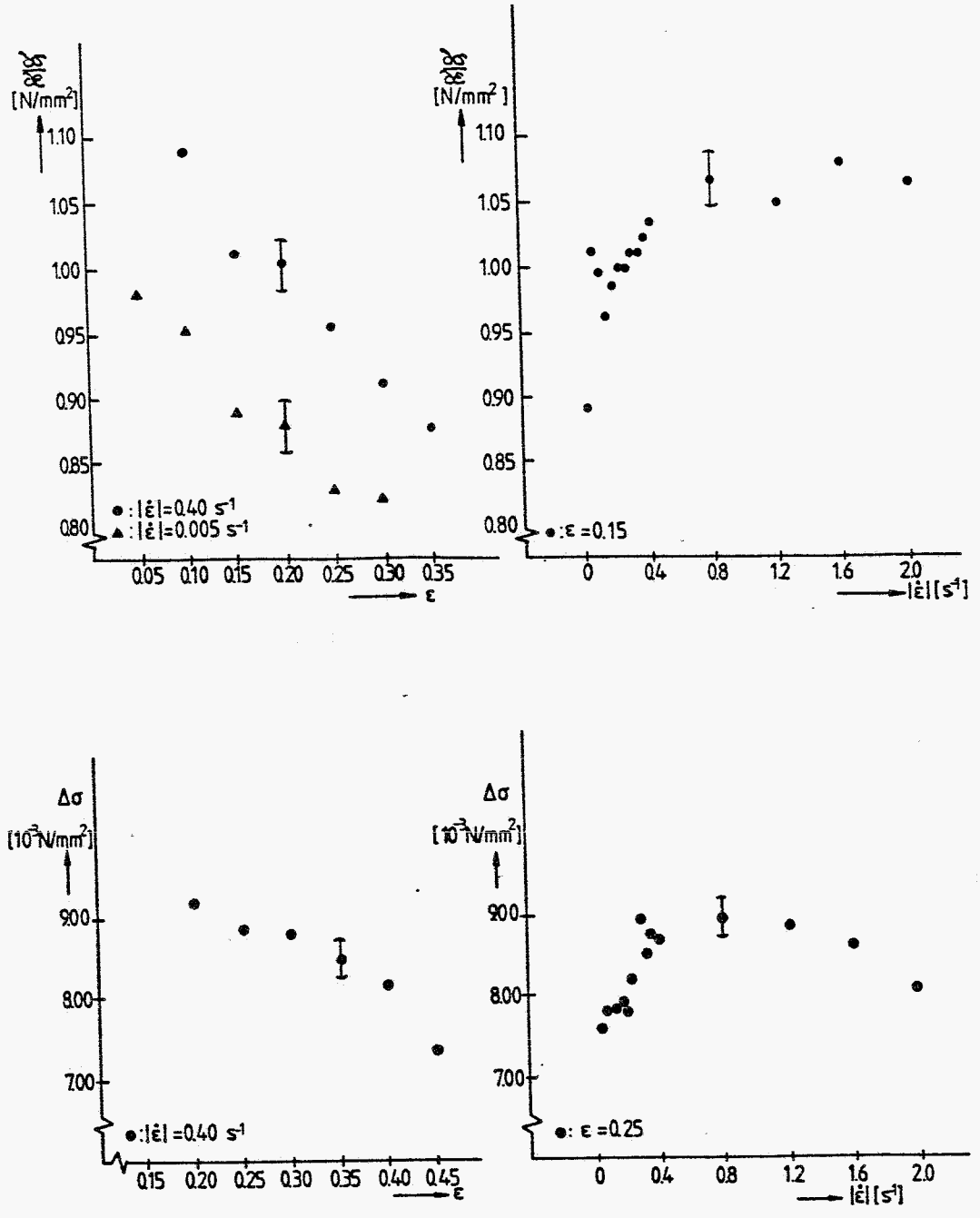

Fig. 4: Relation between the averaged value of the slope of the upward and downward stress-strain curve and the values of a strain and b strain-rate. Analogously the dependency of the stress difference between both curves at a strain corresponding to half the suppressed strain variation as function of c strain and d strain-rate is given.

influence of fluid viscosity. Finally, the pressure signal shows a second rapid increase caused by the wave reflection at the upstream reservoir. In figure 6 one pressure jump is given recorded at two different positions. From this the velocity of wave propagation is estimated to be about 4 m/s. The step-wise shape of the pressure changes observable here, is caused by the transient recorder. In figure 7 a simultaneous recording of the jumps in pressure and diameter 0.22 m. upstream of the valve are given. This illustrates the existing close relationship between area and pressure changes and is used to determine the pressure-volume relationship of the tube during and over the jump. In figure 8 the pressure wave is shown as function of position. The first wave form is close to the valve, the remaining upstream of it at different positions. From these wave forms it is seen that they flatten when travelling upstream and that consequently the rise-time of the pressure jump increases with position. Non-linearities and wall viscosity are thought to be here the dominant factors. Furthermore, the pressure jump appears to decrease slightly while propagating upstream. Probably, this is caused by the influence of fluid viscosity. Finally, some characteristic wave-reflection results are given in figure 9. In the right hand tracing of the upper half the pressure jump close to the valve is given in case of a more compliant "sinus" section than "aortic" one. As a reference in the left half the pressure jump in a uniform tube is given. Due to the compliant "sinus" region the rise time of the pressure close to the valve is found to be increased. Similarly in the lower half the pressure jump is given in case the "sinus" is less compliant than the "aorta". Then pressure oscillations close to the valve are observed. In the next section some physical models will be treated to describe these experimental observations.

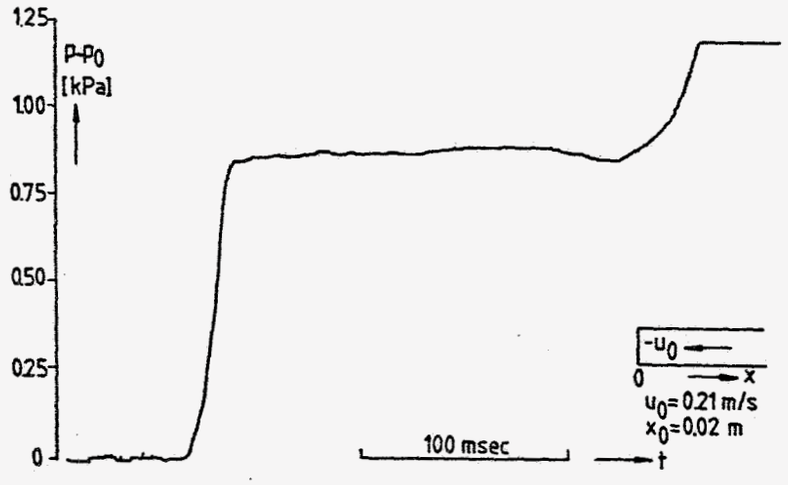

Fig. 5: Typical tracing of the pressure jump measured close to the valve.

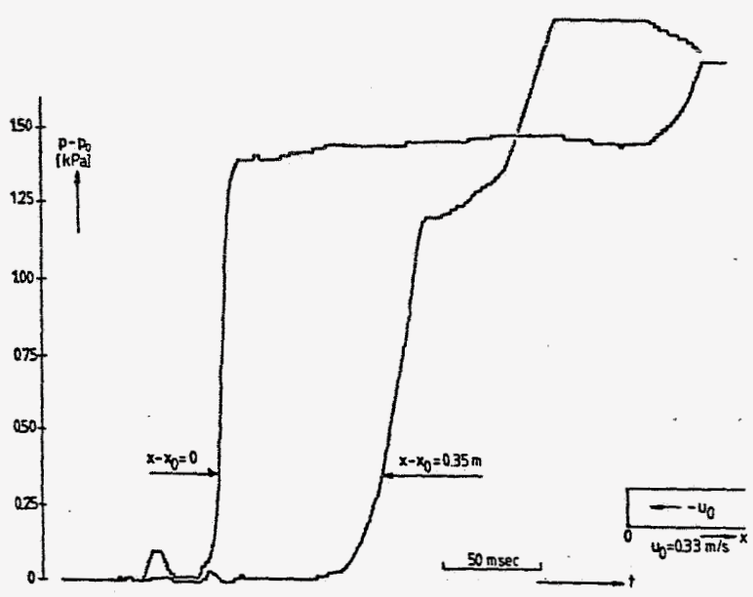

Fig. 6: Recording of the pressure jump at two positions: close to the valve and at the upstream end of the tube.

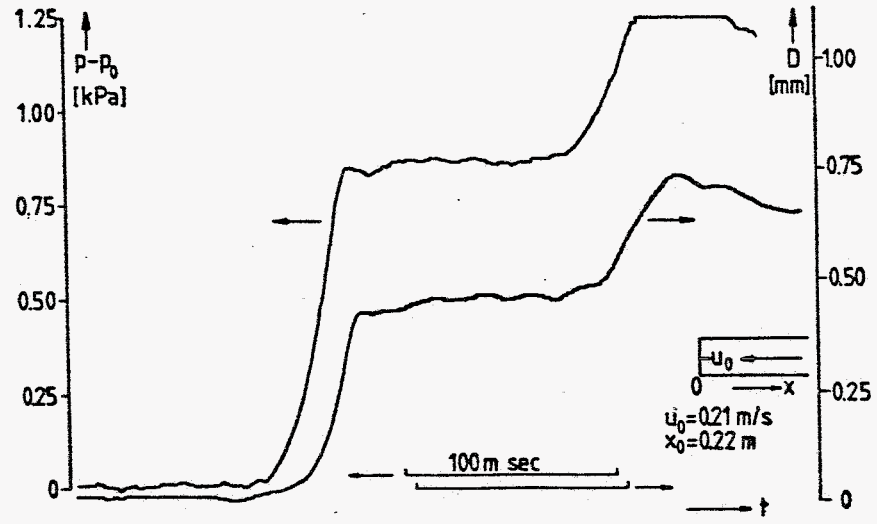

Fig. 7: Simultaneous recording of the jumps in pressure and diameter halfway the tube.

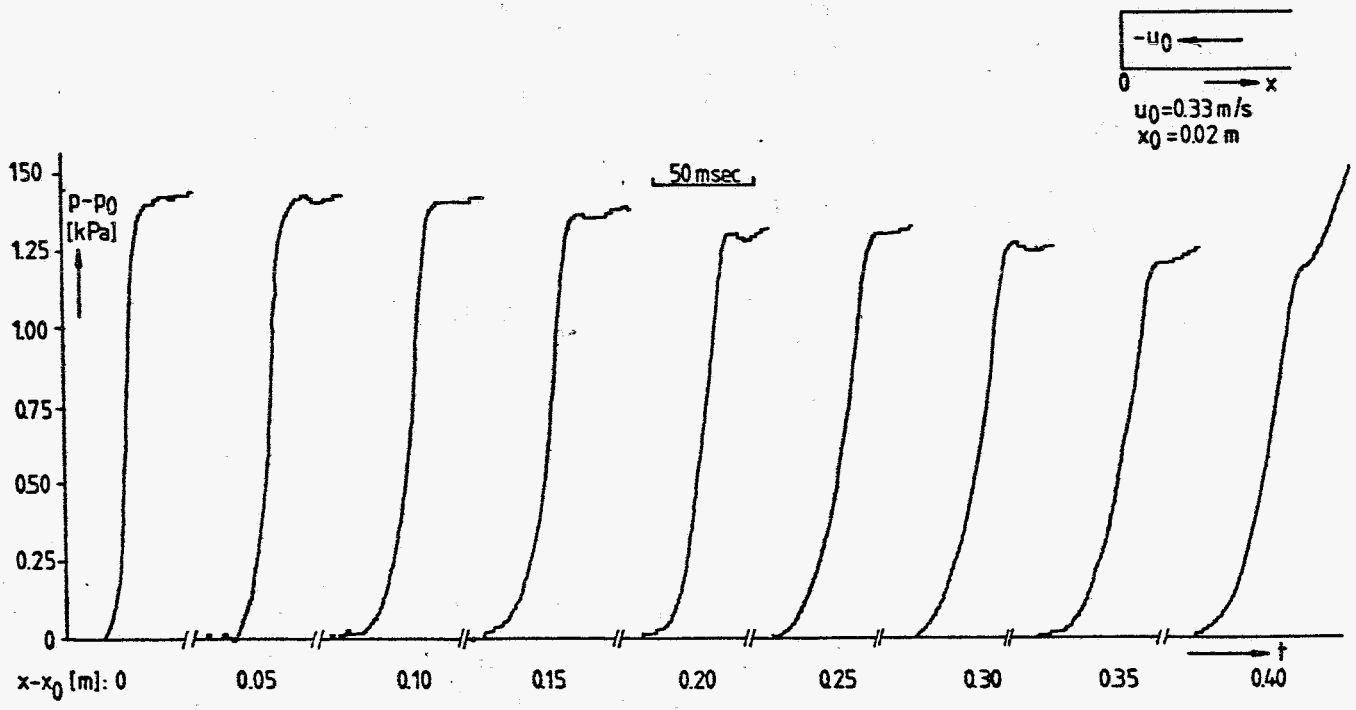

Fig. 8: The pressure wave form as function of position.

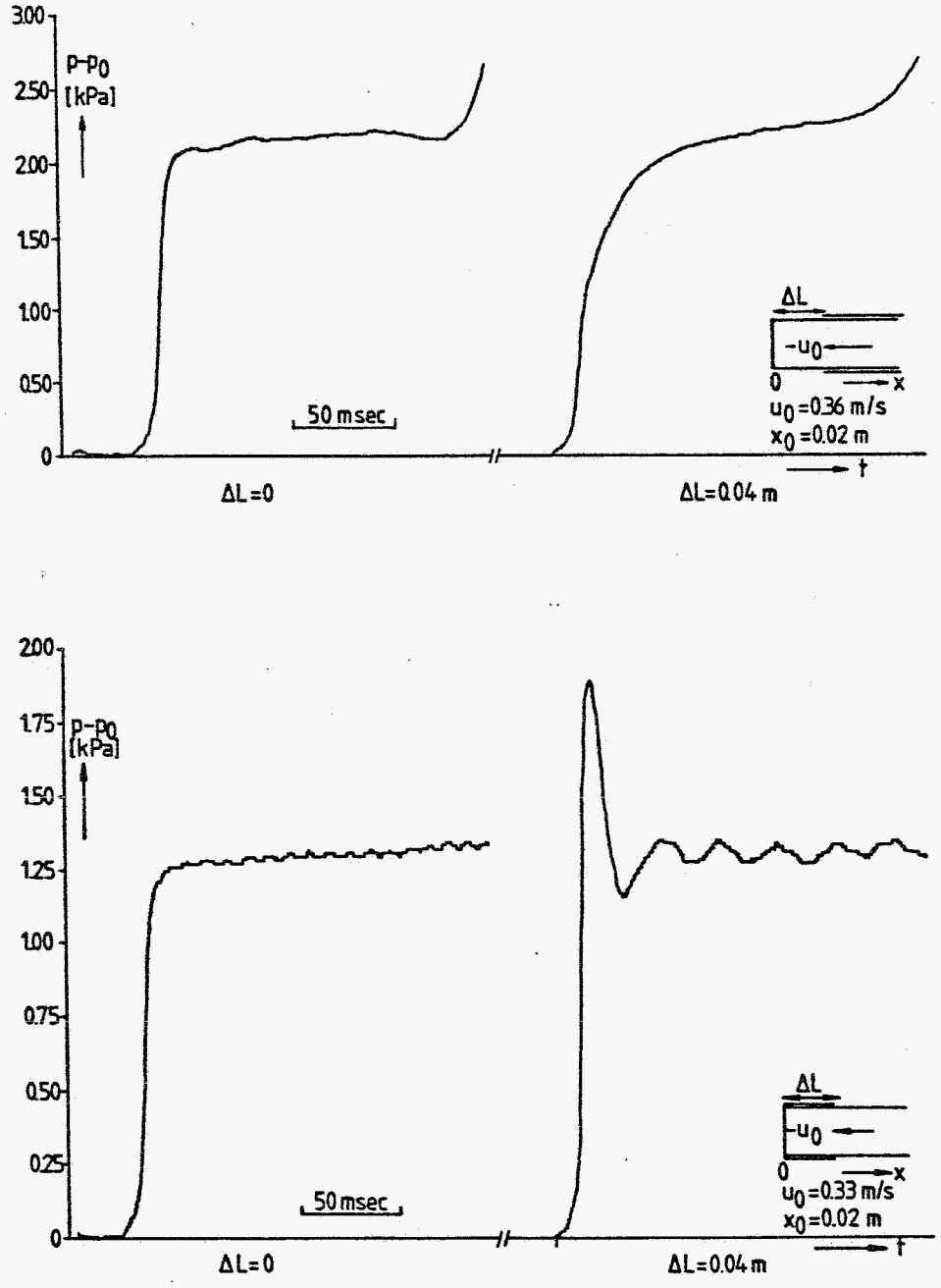

Fig. 9: The influence of the "sinus" compliance in cases of a, b more compliant and c, d less compliant "sinus" section than the remaining tube.

Physical models.

Basic equations.

The observed wave phenomena can mathematically be described by the one-dimensional laws of mass and momentum for a straight uniform flexible tube, see Lighthill (1978) and Pedley (1978). Starting from the continuity equation and the axial component of the Navier-Stokes equation in cylindrical coordinates:

$$1a \qquad \frac{\partial u}{\partial x} + \frac{1}{r}\frac{\partial}{\partial r}(rv) = 0$$

$$1b \qquad \frac{\partial u}{\partial t} + u\frac{\partial u}{\partial x} + v\frac{\partial u}{\partial r} = -\frac{1}{\varrho}\frac{\partial p}{\partial x} + \frac{\eta}{\varrho}\frac{\partial}{\partial r}(r\frac{\partial u}{\partial r})$$

they read after integration over the cross-sectional area and using the kinematic boundary condition:

$$2a \qquad \frac{\partial}{\partial x}(\bar{u}A) + \frac{\partial A}{\partial t} = 0$$

$$2b \qquad \frac{\partial \bar{u}}{\partial t} + \bar{u}\frac{\partial \bar{u}}{\partial x} + \frac{1}{A}\frac{\partial}{\partial x}\{A(\overline{u^2}-\bar{u}^2)\} = -\frac{1}{\varrho}\frac{\partial \bar{p}}{\partial x} + \frac{1}{\varrho}(p_R-\bar{p})\frac{\partial A}{\partial x} + \frac{2\tau}{\varrho R}$$

Here $\bar{u}$, $\bar{p}$ denote the cross-sectional average of axial velocity and pressure, v is the radial velocity; x and r are axial and radial coordinates; t is time; η and ϱ are viscosity and density of the fluid; $\tau = \eta \left.\frac{\partial u}{\partial r}\right|_R$ is the wall shear stress and $A = \pi R^2$ is the cross-sectional area. Usually equation 2b is further reduced by stating:

$$3 \qquad \bar{u}^2 = \overline{u^2} \quad ; \; p_R = \bar{p}$$

After omitting the average symbols the set of equations 2 then obtains its familiar form:

$$4a \qquad \frac{\partial}{\partial x}(uA) + \frac{\partial A}{\partial t} = 0$$

$$4b \qquad \frac{\partial u}{\partial t} + u\frac{\partial u}{\partial x} + \frac{1}{\varrho}\frac{\partial p}{\partial x} = \frac{2\tau}{\varrho R}$$

The assumption of one-dimensionality leading to equation 4 holds if the wave lengths of all disturbances of interest are long compared to the diameter.

In our case the main wave length associated with the axial extent of the wave front is estimated to be about six times the tube diameter. Besides, the neglection of the difference between $\bar{u}^2$ and $\overline{u^2}$ in equation 3 is reasonable when the velocity profile is flat with thin boundary layers outside it, as for the turbulent flow situation before valve closure. After valve closure however, the profile will break down by viscous diffusion as shown by Weinbaum and Parker (1975). The radial pressure variation is quite obviously more or less constant far before and after the wave front. Within the front however, small deviations of p_R from the pressure at the centerline of the tube of the order of 5% are possible. We will assume here that the phenomena observed are well described by the set of equations 4.

In order to describe the wall behaviour we follow Kivity and Collins (1974) by introducing the following tube wall:

$$5 \qquad p = f(A) + g(A)\,\frac{\partial A}{\partial t}$$

Now we define the compliance per unit length c, the wave speed a and a new variable v:

$$6 \qquad c^{-1} = \frac{\partial f}{\partial A} \quad , \quad a^2 = \frac{A}{\varrho c} \quad \text{and} \quad v = \int_{A_0}^{A} \frac{a}{A}\, dA$$

Inserting these definitions in eqs.4, and after some rearrangement we obtain the following characteristic set:

$$7 \qquad \left(\frac{\partial}{\partial t} + (u \pm a)\frac{\partial}{\partial x}\right)(u \pm v) = -\frac{1}{\varrho}\left(\frac{\partial q}{\partial A}\frac{\partial A}{\partial t}\frac{\partial A}{\partial x} + g\,\frac{\partial^2 A}{\partial x \partial t}\right) + \frac{T}{\varrho}$$

The + signs refer to the right running characteristics (c^+), while the - signs refer to the left running characteristics (c^-). The force T equals $\frac{2\tau}{R}$. We shall assume that T is some function of velocity u. Besides, one of the equations 7 can also be used in combination with the continuity equation:

$$8 \qquad \frac{\partial v}{\partial t} + u\,\frac{\partial v}{\partial x} + a\,\frac{\partial u}{\partial x} = 0$$

This set of equations needs to be completed with the initial and boundary conditions:

9a $\quad t \leq 0 \quad : u = -u_0 \quad , p = p_0 = p_{ref} + T_0 x$

9b $\quad x = 0, \; t \geq 0 \; : u = U(t)$

The subscript 0 will represent the initial state.

We shall now consecutively discuss the non-linear inviscid solution, some aspects of wall shear stress, the influence of wall viscosity and reflections due to tube inhomogeneities. For the sake of simplicity and clearness each of these effects will be treated separately. The treatment of non-linear effects is described e.g. by Pedley (1978), while the effects of wall shear stress and wall viscosity are treated on the basis of wave coordinates according to Whitham (1974).

Non-linear inviscid case.
Neglecting shear stresses and wall viscosity, eqs. 7 read:

10 $\quad (\frac{\partial u}{\partial t} + (u \pm a)\frac{\partial}{\partial x})(u \pm v) = 0$

while v can be rewritten as:

11 $\quad v = \int_{p_0}^{p} \frac{1}{\rho a} \, dp$

The initial condition is then $u = -u_0$, $v = 0$ for $t \leq 0$ and the boundary condition at $x = 0$ is $u = 0$ for $t \geq 0$. Applying the invariance of $u - v$ to the points A and B of fig. 10 we obtain:

12 $\quad v_B = u_0$

We can approximate v, defined by eq. 11, by assuming a linear relation between a and p:

13 $\quad a = a_0(1 - \alpha(p-p_0))$

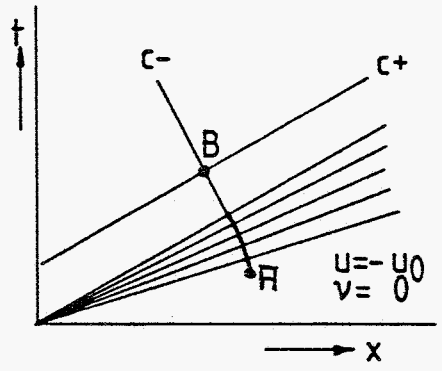

Fig. 10: x-t diagram in case of non-linear elastic tube behaviour.

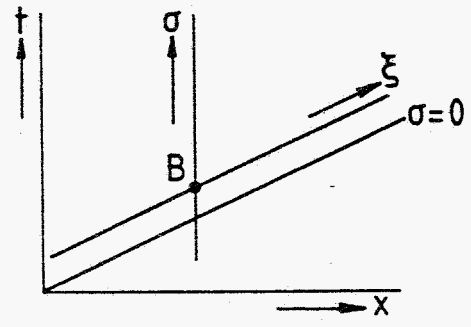

Fig. 11: Introduction of the wave-coordinates ξ and σ.

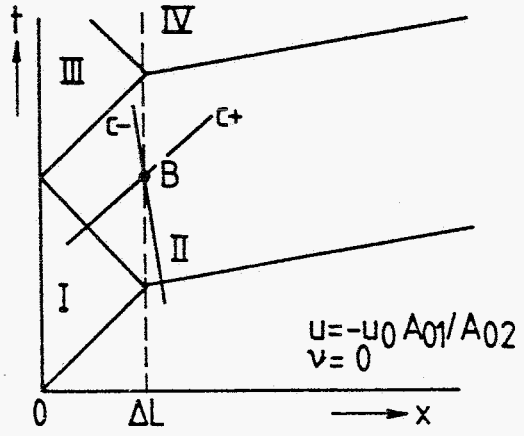

Fig. 12: x-t diagram in case of a tube inhomogeneity.

with $\alpha(p-p_0) << 1$. Then:

$$14 \qquad v = \frac{1}{\varrho a_0}\{(p-p_0) + \frac{1}{2}\alpha(p-p_0)^2\}$$

and the solution for the jump in pressure becomes:

$$15 \qquad p_B - p_0 = \varrho a_0 u_0 (1 - \frac{1}{2}\alpha\varrho a_0 u_0)$$

For the latex tube $\alpha > 0$, so the jump becomes smaller due to the non-linearity.

There is a second effect of importance. The front of the wave travels with velocity $(-u_0+a_0)$ upstream. The tail of the wave however, travels with velocity (u_B+a_B) which equals $a_0(1-\alpha(p_B-p_0))$ according to eq. 13. With eq. 15 the tail wave velocity becomes approximately $a_0-\alpha\varrho a_0^2 u_0$, which is larger than the front velocity for $\alpha\varrho a_0^2 > 1$. More generally spoken the wave form travels with velocity

$$16 \qquad \frac{\Delta x}{\Delta t} = a + u$$

As for each point of the wave form:

$$17 \qquad u - v = -u_0$$

we then find to first order in $p-p_0$ from eqs. 13 and 14:

$$18 \qquad \frac{\Delta x}{\Delta t} = a_0\{1 + (p-p_0)(\frac{1}{\varrho a_0^2} - \alpha)\} - u_0$$

The wave front center, defined as that particular point where $p-p_0 = \frac{1}{2}(p_B-p_0)$, travels with velocity:

$$19 \qquad (\frac{\Delta x}{\Delta t})_c = a_0(1 - \frac{1}{2}\frac{u_0}{a_0} - \frac{1}{2}\alpha\varrho a_0 u_0)$$

From eq. 10 it follows that the wave travels undistorted for $\alpha\varrho a_0^2 = 1$ as already pointed out by Olsen and Shapiro (1967), while for the special case of $\alpha = 0$ the wave would steepen. In our case $\alpha\varrho a_0^2$ is somewhat larger than 1 and

a slightly decreasing slope is expected. Assuming an instantaneous jump of the pressure at x = 0, the rise time of the pressure at position x will be:

$$20 \qquad \Delta t = x \left(\frac{1}{u_B+a_B} - \frac{1}{-u_0+a_0}\right) = \left(\alpha\varrho - \frac{1}{a_0^2}\right)u_0 x$$

Finally we consider the influence of initial pressure p_0 on wave front velocity, by raising p_0 with regard to a reference pressure p_{ref}. Again we assume $\alpha(p_0-p_{ref}) \ll 1$ and

$$21 \qquad a_0 = a_{ref}(1 - \alpha(p_0-p_{ref}))$$

To first order in pressure we then find for the velocity of the wave front center:

$$22 \qquad \left(\frac{\Delta x}{\Delta t}\right)_c = a_{ref}\left\{1 - \frac{1}{2}\frac{u_0}{a_{ref}} - \alpha\left(\frac{1}{2}\varrho a_{ref}u_0 + (p_0-p_{ref})\right)\right\}$$

Some aspects of wall shear stress.

For the linear, pure elastic situation the equation set 7 using eq. 11 reduces to

$$23 \qquad \left(\frac{\partial}{\partial t} \pm a_0 \frac{\partial}{\partial x}\right)\left(u \pm \frac{p}{\varrho a_0}\right) = \frac{T}{\varrho}$$

The corresponding initial and boundary conditions read:

$$24a \qquad u = -u_0 \quad \text{and} \quad \frac{\partial p}{\partial x} = T_0 \quad \text{or} \quad p_0 = p_{ref} + T_0 x \quad \text{for } t \to -\infty$$

$$24b \qquad u = u_v(t) \quad \text{at} \quad x = 0$$

In order to analyse the problem we shall introduce the following wave coordinates (see figure 11):

$$25 \qquad \xi_1 = \frac{T_0}{\varrho u_o a_0} x \quad \text{and} \quad \sigma = (a_0 t - x)/a_0 t_0$$

where t_0 is a characteristic time for valve closure. The dimensionless time σ has to be interpreted as the time elapsed since the passage of the wave front on a fixed x position. Further we shall assume that the wall shear stress is a function of velocity only, which vanishes for zero velocity:

26 $$T = T(u) \quad , \quad T(0) = 0$$

Finally we introduce reduced values for u, v and T:

27 $$\hat{u} = \frac{u}{u_0} \quad , \quad \hat{v} = \frac{p}{\varrho a_0 u_0} \quad , \quad \hat{T} = \frac{T}{T_0}$$

Then eq. 23 for the right running characteristic becomes:

28 $$\frac{\partial}{\partial \xi_1}(\hat{u} + \hat{v}) = \hat{T}$$

As a second equation it is useful to rewrite the linearised version of eq. 8:

29a $$\frac{\partial v}{\partial t} + a_0 \frac{\partial u}{\partial x} = 0$$

in terms of the new variables:

29b $$\frac{\partial \hat{v}}{\partial \sigma} - \frac{\partial \hat{u}}{\partial \sigma} = - \varepsilon_1 \frac{\partial \hat{u}}{\partial \xi_1}$$

where we have defined the small parameter ε_1 as:

30 $$\varepsilon_1 = \frac{T_0 t_0}{\varrho u_0}$$

The initial and boundary conditions in terms of the new variables are:

31a $$\hat{u} = - 1, \quad \hat{v} = \xi_1 \qquad \text{for } \sigma \to -\infty$$

31b $$\hat{u} = \hat{u}_v(\sigma) \text{ for } \xi_1 = 0$$

Now $\hat{v}$, $\hat{u}$ and $\hat{T}$ are expanded in the small parameter ε

$$\hat{u} = \hat{u}^{(0)} + \varepsilon_1 \hat{u}^{(1)} + \ldots, \quad \hat{v} = \hat{v}^{(0)} + \varepsilon_1 \hat{v}^{(1)} + \ldots, \quad \hat{T} = \hat{T}^{(0)} + \varepsilon_1 \hat{T}^{(1)} + \ldots$$

This series expansion will be valid under the condition $\varepsilon_1 \sigma << 1$.
After a substitution of this expansion in eqs. 28 and 29b and after equating terms with equal powers of ε we obtain:

32a $$\frac{\partial}{\partial \sigma}(\hat{v}^{(0)} - \hat{u}^{(0)}) = 0$$

32b $$\frac{\partial}{\partial \xi_1}(\hat{v}^{(0)} + \hat{u}^{(0)}) = \hat{T}^{(0)}$$

33a $$\frac{\partial}{\partial \sigma}(\hat{v}^{(1)} - \hat{u}^{(1)}) = - \frac{\partial \hat{u}^{(0)}}{\partial \xi_1}$$

33b $$\frac{\partial}{\partial \xi_1}(\hat{v}^{(1)} + \hat{u}^{(1)}) = \hat{T}^{(1)}$$

These equations cannot be solved without further specifying the functional relationship $\hat{T}(\hat{u})$. However it is possible to derive a property for the pressure at the valve which has a rather general validity. To that end we integrate eq. 32a, making use of condition 31a:

34 $$\hat{v}^{(0)} = \hat{u}^{(0)} + 1 + \xi_1$$

After substitution of this result in 32b we find:

35 $$\frac{\partial}{\partial \xi_1}\hat{u}^{(0)} = \frac{1}{2}(\hat{T}^{(0)} - 1)$$

This can be used in 33a for the first order disturbances:

36 $$\frac{\partial}{\partial \sigma}(\hat{v}^{(1)} - \hat{u}^{(1)}) = - \frac{1}{2}(\hat{T}^{(0)} - 1)$$

Applying this to the valve, where $\hat{u}^{(1)} = 0$ we find:

37 $$\hat{v}^{(1)} = - \frac{1}{2} \int_{-\infty}^{\sigma} (\hat{T}^{(0)} - 1) d\sigma'$$

Rewriting this in the orginal physical quantities we find:

38 $$p = \varrho a_0 \{u_v(t) + u_0\} + \frac{1}{2} a_0 \int_{-\infty}^{t} (-T_0^{(0)} + T_0)dt'$$

This means that after complete valve closure when $T^{(0)}(0) = 0$, the pressure steadily increases with a rate proportional to the initial wall shear stress T_0. It is remarked again that the solution is only valid for $\varepsilon_1 \sigma << 1$.

In order to proceed further, we shall distinguish two different cases for the velocity dependence of $\hat{T}$:

case i:

39 $$\hat{T} = - \hat{u}$$

Now the solution of eq. 35 becomes:

40a $$\hat{u}^{(0)} = (\hat{u}_v(\sigma) + 1)\, e^{-\xi_1/2} - 1$$

and from eq. 34 it follows:

40b $$\hat{v}^{(0)} = \xi_1 + (\hat{u}_v(\sigma) + 1)\, e^{-\xi_1/2}$$

Since $\hat{u}_v(\sigma)$ varies from -1 to 0, the total change in $v^{(0)}$ across the wave equals:

41a $$\Delta\hat{v}^{(0)} = e^{-\xi_1/2}$$

and the rate of change at the wave front center (σ=0) reads

41b $$\left(\frac{\partial \hat{u}^{(0)}}{\partial \sigma}\right)_{0,\xi_1} = \left(\frac{\partial \hat{v}^{(0)}}{\partial \sigma}\right)_{0,\xi_1} = \left(\frac{\partial \hat{u}_v}{\partial \sigma}\right)_0 e^{-\xi_1/2}$$

The characteristic length scale for the exponential decay of the jump appears to be, referring to the definition of ξ_1:

42 $$L_1 = \frac{2\varrho u_0 a_0}{T_0}$$

The solution for $\hat{v}^{(1)}$ and $\hat{u}^{(1)}$ is found by integration of eqs. 36 and 37 subject to the condition that $\hat{v}^{(1)}$ and $\hat{u}^{(1)}$ both vanish as $\sigma \to -\infty$. The result is, see appendix:

43a $$\hat{u}^{(1)} = \frac{1}{8} \hat{I}_v(\sigma)\, \xi_1\, e^{-\xi_1/2}$$

43b $$\hat{v}^{(1)} = \frac{1}{2} \hat{I}_v(\sigma) e^{-\xi_1/2} \{1 + \frac{1}{4} \xi_1\}$$

with $\hat{I}_v = \int_{-\infty}^{\sigma} (1 + \hat{u}_v)\, d\sigma'$

<u>case ii</u>:

44 $$\hat{T} = - \hat{u}|\hat{u}|$$

Since in the present situation $|\hat{u}| = -\hat{u}$, we can take $\hat{T} = \hat{u}^2$. In that case eq. 35 becomes

45 $$\frac{\partial}{\partial \xi_1} \hat{u}^{(0)} - \frac{1}{2} \hat{u}^{(0)2} = - \frac{1}{2}$$

with solution $(\tanh)^{-1} \hat{u}^{(0)} = (\tanh)^{-1} \hat{u}_v(\sigma) - \frac{1}{2} \xi_1$. Again, since $\hat{u}_v(\sigma)$ varies from -1 at $\sigma \to -\infty$ to 0 after valve closure, the total jumps in velocity and "pressure" are:

46 $$\Delta \hat{u}^{(0)} = \Delta \hat{v}^{(0)} = + \tanh(\frac{1}{2} \xi_1)$$

The influence of wall viscosity.

The effects of wall viscosity can be treated in a similar way as that of wall shear stress. As starting eqs. we take the linearised inviscid version of eq. 7 for the right running characteristic and the equation of continuity of mass, eq. 29a:

47a $$(\frac{\partial}{\partial t} + a_0 \frac{\partial}{\partial x})(u + v) = - \frac{g_0}{\varrho} \frac{\partial^2 A}{\partial x \partial t}$$

47b $$\frac{\partial v}{\partial t} + a_0 \frac{\partial u}{\partial x} = 0$$

Since $v = \frac{a_0}{A_0}(A-A_0)$ it is possible to rewrite the right hand side of eq. 47a with 47b:

48 $$\frac{\partial^2 A}{\partial x \partial t} = - A_0 \frac{\partial^2 u}{\partial x^2}$$

Let σ and ξ_2 be the new independent coordinates, which are defined as:

49 $$\sigma = (a_0 t - x)/a_0 t_0 \quad \text{and} \quad \xi_2 = \frac{g_0 A_0}{\varrho a_0^3 t_0^2} x$$

Then eqs. 47 can be written, using eq. 48 as:

50 $$\frac{\partial}{\partial \sigma}(\hat{u} - \hat{v}) = \varepsilon_2 \frac{\partial \hat{u}}{\partial \xi_2}$$

$$\frac{\partial}{\partial \xi_2}(\hat{u} + \hat{v}) = \frac{\partial^2 \hat{u}}{\partial \sigma^2} - 2\varepsilon_2 \frac{\partial^2 \hat{u}}{\partial \sigma \partial \xi_2} + \varepsilon_2^2 \frac{\partial^2 \hat{u}}{\partial \xi_2^2}$$

with

51 $$\varepsilon_2 = \frac{g_0 A_0}{\varrho a_0^2 t_0}$$

Expanding the solution for $\hat{u}$ and $\hat{v}$ in powers of ε_2 and equating terms of zeroth order in ε_2 yields, under the condition $\varepsilon_2 \sigma << 1$

52a $$\frac{\partial}{\partial \sigma}(\hat{u}^{(0)} - \hat{v}^{(0)}) = 0$$

52b $$\frac{\partial}{\partial \xi_2}(\hat{u}^{(0)} + \hat{v}^{(0)}) = \frac{\partial^2 \hat{u}^{(0)}}{\partial \sigma^2}$$

The solution of eq. 52a with initial condition $\hat{u}^{(0)} \to -u_0$ and $\hat{v}^{(0)} \to 0$ as $\sigma \to -\infty$ is:

53 $$\hat{v}^{(0)} = \hat{u}^{(0)} + 1$$

So, eq. 52b becomes the ordinary diffusion equation:

54 $$\frac{\partial \hat{u}^{(0)}}{\partial \xi_2} = \frac{1}{2} \frac{\partial^2 \hat{u}^{(0)}}{\partial \sigma^2}$$

If we represent the boundary condition $\hat{u}_v(\sigma)$ by the following form:

55 $$\hat{u}_v(\sigma) = -\frac{1}{2} \operatorname{erfc}\left(\frac{\sigma}{\sqrt{2\xi_0}}\right)$$

the solution of eq. 54 becomes:

56 $$\hat{u}^{(0)} = -\frac{1}{2} \operatorname{erfc}\left(\frac{\sigma}{\sqrt{2(\xi_2+\xi_0)}}\right)$$

This solution illustrates the gradual broadening of the wave front due to wall viscosity. The time derivative of velocity and of v at the wavefront center, $\sigma = 0$, are:

57 $$\left(\frac{\partial \hat{u}^{(0)}}{\partial \sigma}\right)_{0,\xi_2} = \left(\frac{\partial \hat{v}^{(0)}}{\partial \sigma}\right)_{0,\xi_2} = \{2\pi(\xi_2 + \xi_0)\}^{-\frac{1}{2}}$$

Hence it follows that ξ_0 can be interpreted in terms of the maximum rate of change of the velocity at the valve:

58 $$\xi_0 = \frac{1}{2\pi}\left(\frac{d\hat{u}_v}{d\sigma}\right)_0^{-2}$$

With this definition of ξ_0 eq. 57 rewritten in the original variables becomes:

59 $$\left(\frac{\partial u^{(0)}}{\partial t}\right)_{max} = \left(\frac{du_v}{dt}\right)_0 \{1 + \frac{2\pi\left(\frac{du_v}{dt}\right)_0^2 g_0 A_0}{a_0^3 u_0^2 \rho} x\}^{-\frac{1}{2}}$$

An expression for the rate of change of the pressure follows from eqs. 5 and 6 in linearised form:

60 $$\frac{\partial p}{\partial t} = \rho a_0 \frac{\partial v}{\partial t} + g_0 \frac{A_0}{a_0} \frac{\partial^2 v}{\partial t^2}$$

Then $\left(\frac{\partial p}{\partial t}\right)_{max} = \rho a_0 \left(\frac{\partial u^{(0)}}{\partial t}\right)_{max}$, since $\frac{\partial^2 v}{\partial t^2}$ is zero at the wave front center.

The solution for $\hat{v}^{(1)}$ at the valve is quite easily obtained by substituting expression 56 for $\hat{u}^{(0)}$ in the first order equation:

61a $$\frac{\partial}{\partial \sigma}\{\hat{u}^{(1)} - \hat{v}^{(1)}\} = \frac{\partial \hat{u}^{(0)}}{\partial \xi_2}$$

and taking into account that $\hat{u}^{(1)}$ is 0 at $\xi_2 = 0$. We then find for $v^{(1)}$:

61b $$\hat{v}^{(1)}_{0,\xi_2} = \frac{1}{2\sqrt{2\pi\xi_0}} e^{-\frac{\sigma^2}{2\xi_0}}$$

The solution is accurate if $\varepsilon_2 \sigma << 1$. So wall viscosity does not modify the final valve of $\hat{v}^{(1)}$ after the jump.

Wave-reflections.

Suppose two regions of different wall properties and cross-sectional areas and assume that the change of properties occurs in a distance l satisfying the compactness condition (Lighthill 1978):

62 $$\frac{l}{a_{0i} t_0} << 1 \qquad , i = 1,2$$

The inviscid, elastic and linearised equations 7 read:

63 $$(\frac{\partial}{\partial t} \pm a_{0i} \frac{\partial}{\partial x})(u_i \pm \frac{p_i}{\varrho a_{0i}}) = 0 \qquad i = 1,2$$

with

64 $$a_{0i} = (\frac{A_{0i}}{\varrho c_{0i}})^{\frac{1}{2}}$$

The initial and boundary conditions 9 reduce to:

65a $$u_1 = -u_0 \; , \; u_2 = -u_0 A_{01}/A_{02} \; , \; p_i = p_0 \qquad t \leq 0$$

65b $$u_1 = 0 \qquad x = 0 \; , \; t \geq 0$$

Continuity of pressure and flow at the interface ($x = \Delta L$) implies:

66a $$p_1(\Delta L,t) = p_2(\Delta L,t)$$

66b $$u_1(\Delta L,t)A_{01} = u_2(\Delta L,t)A_{02}$$

We further introduce as reflection coefficient:

67 $$R = \frac{Z_2 - Z_1}{Z_2 + Z_1} \qquad \text{with} \quad Z_1 = \frac{\varrho a_{01}}{A_{01}}$$

Combination of a c^+-characteristic in region 1 and a c^--characteristic in region 2 using eq. 66 then directly leads to the pressure solution in the two regions as function of time, see figure 12[d]:

68

t	p_1
$0 \rightarrow \Delta t_1$	p_0
$\rightarrow \Delta t_1+\Delta t_2$	$p_0+\varrho a_{01} u_0$
$\rightarrow 3\Delta t_1+\Delta t_2$	$p_0+(1+R)\varrho a_{01}u_0$
$\rightarrow 3\Delta t_1+2\Delta t_2$	$p_0+(1+2R)\varrho a_{01}u_0$
$\rightarrow 5\Delta t_1+2\Delta t_2$	$p_0+(1+2R+R^2)\varrho a_{01}u_0$
$\rightarrow 5\Delta t_1+3\Delta t_2$	$p_0+(1+2R+2R^2)\varrho a_{01}u_0$

with:

69 $$\Delta t_1 = \frac{x_1}{a_{01}} \quad , \quad \Delta t_2 = 2\frac{(\Delta L - x_1)}{a_{01}}$$

and:

70

t	p_2
$0 \rightarrow \Delta t_3$	p_0
$\rightarrow \Delta t_3+\Delta t_4$	$p_0+(1+R)\varrho a_{01}u_0$
$\rightarrow \Delta t_3+2\Delta t_4$	$p_0+(1+2R+R^2)\varrho a_{01}u_0$

with:

71 $$\Delta t_3 = \frac{\Delta L}{a_{01}} + \frac{x_2-\Delta L}{a_{02}} \quad , \quad \Delta t_4 = \frac{2\Delta L}{a_{01}}$$

The limiting value in both regions is as expected:

72 $$p_1 = \lim_{n\to\infty} [p_0+\varrho a_{01}u_0+2\varrho a_{01}u_0 R(1+R+R^2+\ldots R^n)$$

$$= p_0+\varrho a_{02}u_0 A_{01}/A_{02}$$

Hence a positive reflection coefficient ($Z_1 < Z_2$) causes a gradual increase of the pressure in both regions, while for a negative value of R ($Z_1 > Z_2$) the pressure will oscillatory vary.

Verification of theory

Influence of non-linearities

According to eqs. 15, 19 and 20 the non-linearities affect the pressure height, the velocity of the wave front center and the rise time of the pressure jump at position x. To verify theory, first the material constant α, defined by eq. 13, has to be determined from the pressure dependence of both the cross-sectional area and the compliance per unit length (see eq. 6). Using a screw-micrometer the diameter-pressure relation was measured under quasi-static conditions. From this the area-pressure and compliance-pressure relationships were calculated. The results are given in figure 13. Besides, the simultaneous recorded pressure-diameter changes as for example shown in figure 7 were also used. The compliance per unit-length as determined from the amplitude ratio of diameter and pressure jump are given, as a function of pressure, in figure 13b. This compliance will be denoted as the dynamic one. Finally, figure 14 shows the diameter-pressure relation and the compliance-pressure relation, derived from the former one, during the jump. The differences in the initial values and slopes with those in figure 13 are striking. It is likely that they are a consequence of the visco-elastic properties of the tube wall. Figure 15 shows the corresponding calculated wave speeds together with the values of a_0 and α for the three previous situations.

Next, the pressure height close to the valve was measured as function of the initial velocity, the result of which is given in figure 16. The agreement between theory and experiment is close, especially when the dynamic values of the compliance are used. The dependence of the velocity of the wave front center on the initial velocity is difficult to measure due to the restricted range of adjustable initial velocities. Hence the initial state was changed by raising the initial pressure. The result of this experiment is shown in figure 17, together with the prediction according to eq. 22. Here again the agreement is fair. Finally, the rise-time of the pressure jump, defined by the time interval between 5 and 95% of the amplitude, is determined as function of position from wave forms like those shown in figure 8. Non-linear theory based on the values of both static and dynamic compliances predicts that the wave form would travel almost undistorted which is in contrast with the experimental results, see figure 18. In this figure also the prediction is given based upon the calculated wave speed derived from the

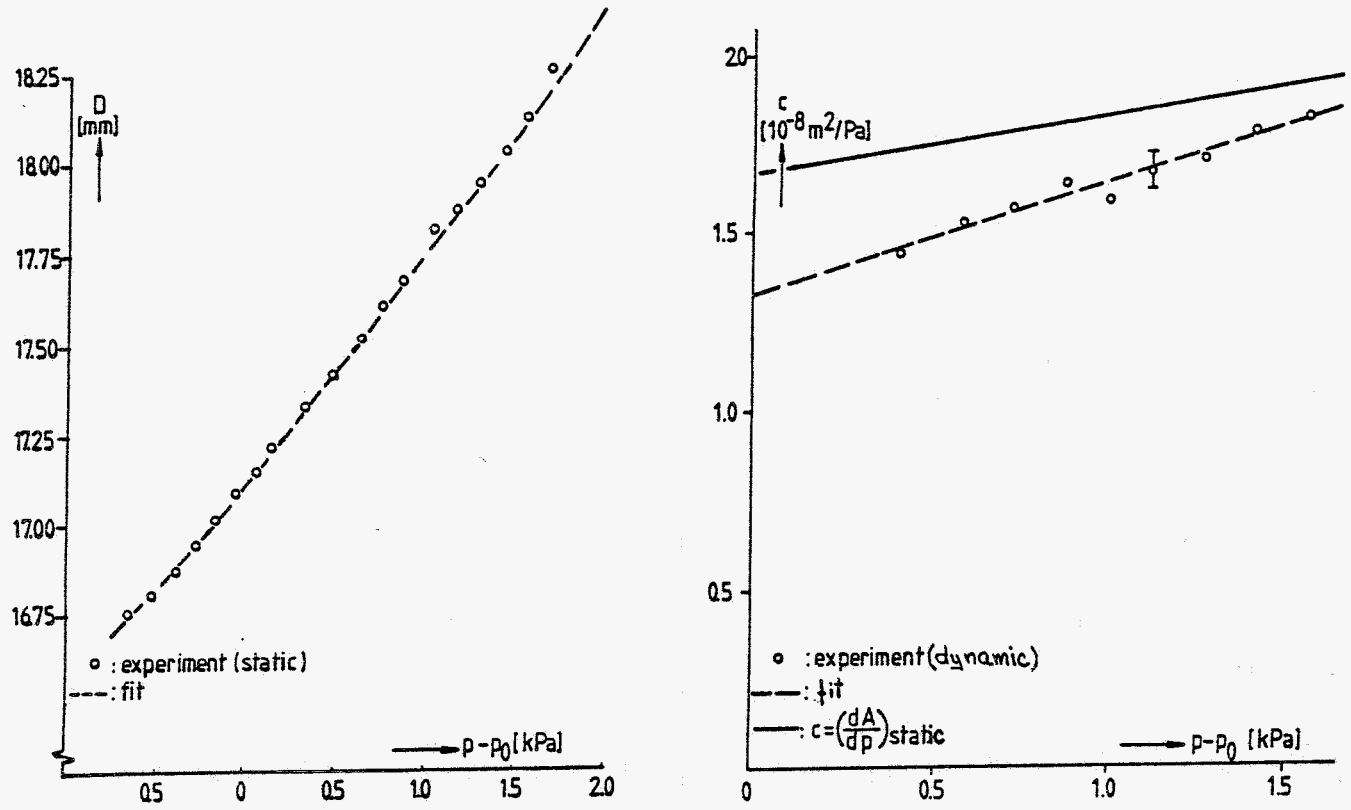

Fig. 13: Relationships over the pressure jump between
a diameter and pressure and b compliance and pressure.
The fitted lines correspond to:
a $D = 17.12\ \{1+0.36\ 10^{-4}(p-p_0) + 0.082\ 10^{-8}(p-p_0)^2\}$, $r^2 = 0.999$.
b $c = 1.33\ 10^{-8}\ \{1+0.23\ 10^{-3}(p-p_0)\}$, $r^2 = 0.952$.

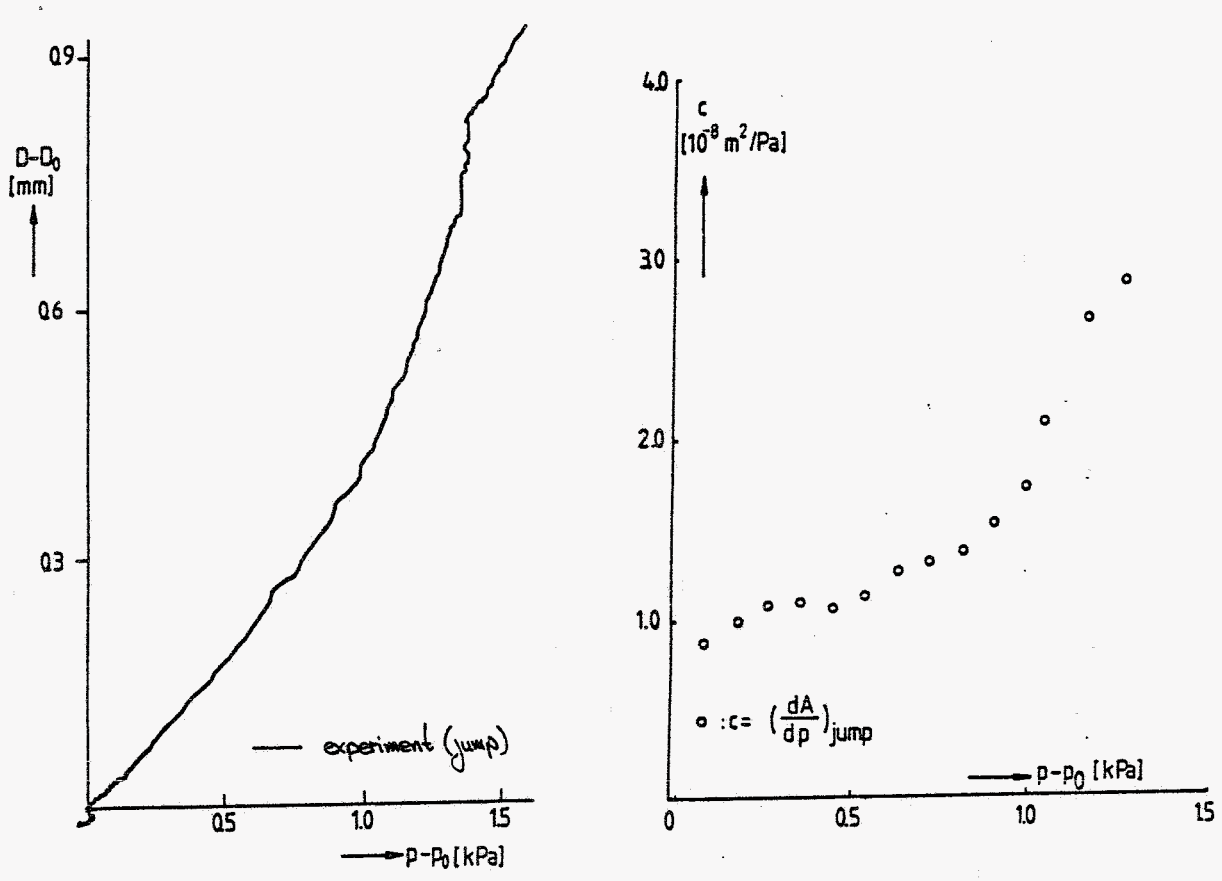

Fig. 14: Relationships during the pressure jump between
a diameter and pressure and b compliance and pressure.

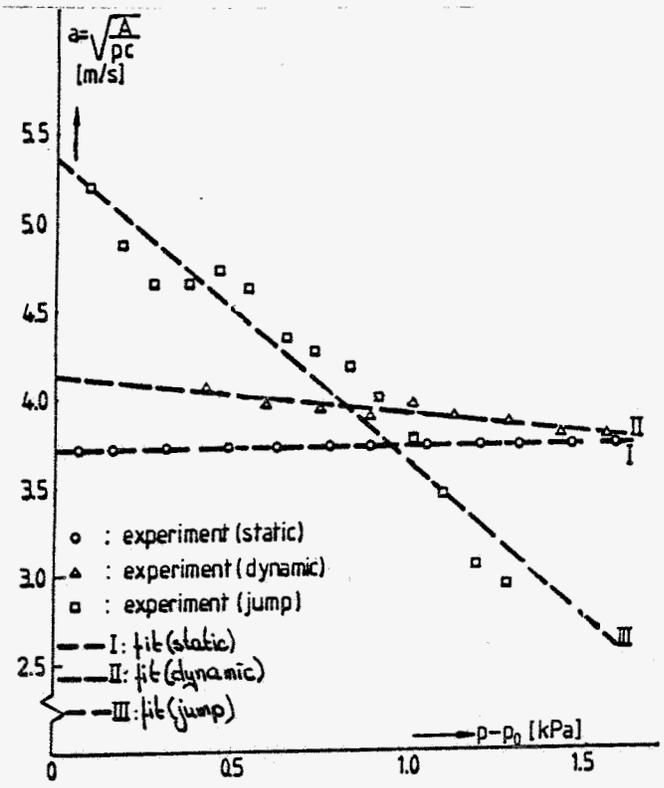

Fig. 15: The wave-speed as function of pressure, calculated from the data of figs. 13 and 14. The fitted lines correspond to:

I: $a = 3.71$

II: $a = 4.11\ \{1-0.53\ 10^{-4}\ (p-p_0)\}$, $r^2 = 0.879$

III: $a = 5.36\ \{1-3.3\ 10^{-4}\ (p-p_0)\}$, $r^2 = 0.935$

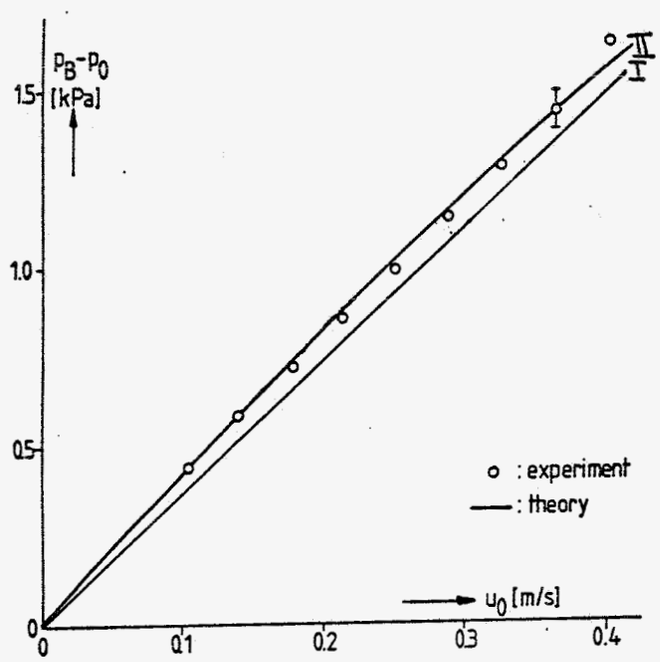

Fig. 16: The amplitude of the pressure jump as function of the initial velocity.

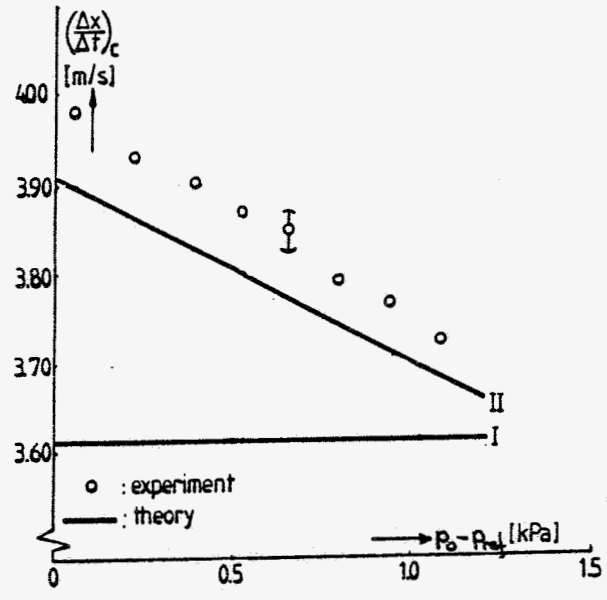

Fig. 17: The velocity of the wave front center as function of the initial pressure.

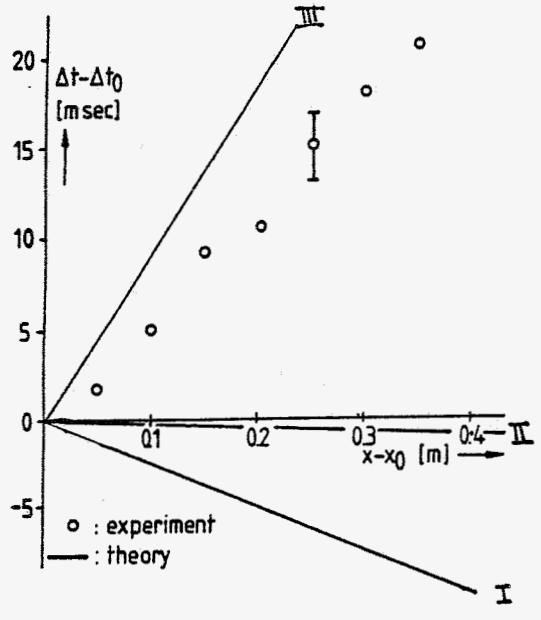

Fig. 18: The rise-time of the pressure jump as function of position.

diameter-pressure relationship during the jump. Although this prediction is quite unaccurate due to the small time interval of measurement (~ 15 msec), the much greater values indicate that the wall viscosity is the dominant cause of the experimentally observed wave front expansion.

Influence of wall shear stress

The main influences of the wall shear stress as predicted from theory are the steadily increase of the pressure after the jump front (eq. 38), the gradual decrease of the height of the pressure jump as function of position (eq. 41a) and a contribution to the wave front expansion (eq. 41b). For all theoretical predictions a value of the initial wall shear stress is necessary. This value was estimated from the turbulent-flow pressure-loss relation (Schlichting, 1979):

$$73 \qquad T_0 = \lambda \frac{1}{2} \frac{\rho u_0^2}{D} \quad \text{with} \quad \lambda = 0.316\ Re^{-0.25}$$

A verification of this relation at the Reynoldsnumbers occuring in our set-up (1800-7200), was performed by the pressure drop measurement over a uniform tube of 80 cm length, the result of which is given in figure 19.

Next, the slope of the pressure after the jump was measured close to the valve as function of the initial velocity. As given in figure 20, theory and experiment show qualitatively the same tendency although theory underestimates the experimental observation considerably. The decrease of the height of the pressure jump as function of position, predicted by theory, is also observed. However, figure 21 illustrates that a much stronger decrease was found than predicted from theory. Both results indicate that the assumed relation 73 underestimates the initial wall shear stress considerably, probably due to the disturbance of pressure-catheters and valve house. Finally, the influence of wall shear stress on the wave front expansion was estimated from eq. 41b to be less than 0.5 msec. Hence wall shear stress is not expected to cause the observed expansion.

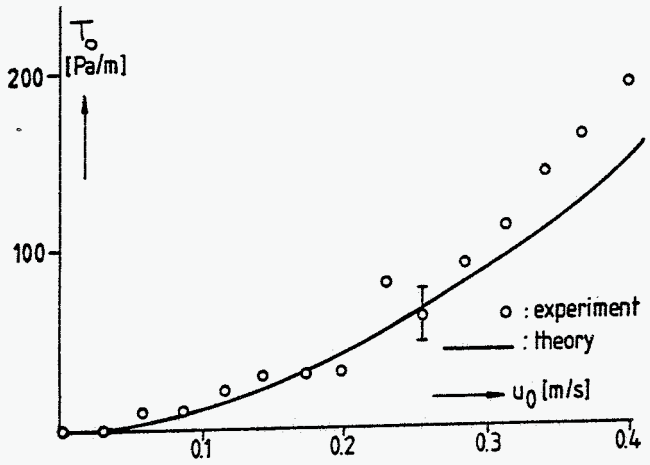

Fig. 19: The initial wall shear stress as function of the initial velocity, determined from the pressure drop over a uniform tube of 80 cm length.

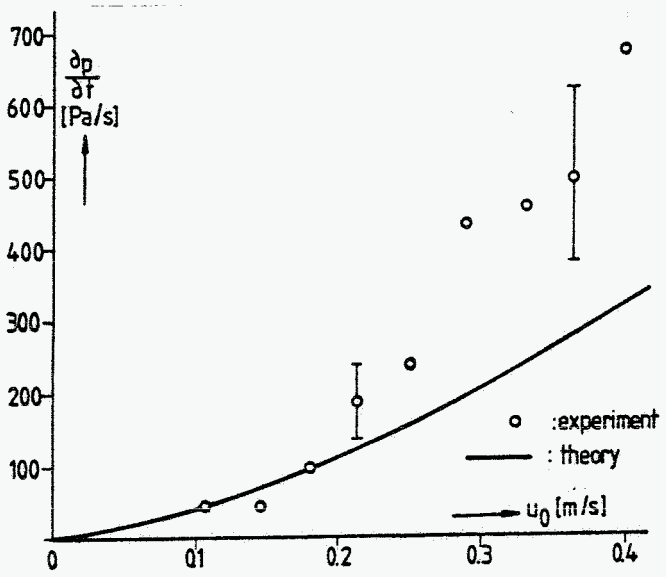

Fig. 20: The slope of the pressure after the jump close to the valve as function of the initial velocity.

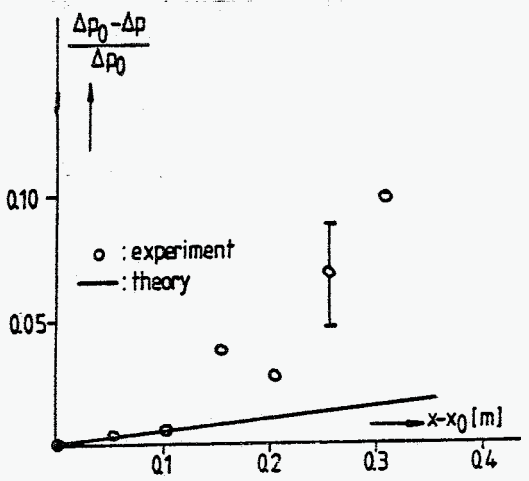

Fig. 21: The decrease of the height of the pressure jump as function of position.

Influence of wall viscosity

The main influence of wall viscosity is expected from experiment to be the expansion of the wave front as function of position. This is justified by the analysis of the simple material model given by eq. 5, leading to eq. 60. From the tensile experiments given in figure 4 the conclusion was drawn that this material model is not appropriate to describe the observed independence of the viscous parameter on the strain-rate value. However, as a very crude approximation we deduce the visco-elastic parameter g_0 of eq. 5 from the measured value of $\Delta\sigma$ given in figure 4d for values of $\dot{\varepsilon}$ of about 2.0 s^{-1}. With $p = \sigma h_0/R_0$ and $\varepsilon = \frac{1}{2}dA/A_0$, where h_0 and R_0 correspond to the initial thickness and radius of the tube, it follows that:

74 $$\frac{\Delta\sigma}{\dot{\varepsilon}} = \frac{4g_0A_0R_0}{h_0}$$

This yields a value for g_0 of 1.0 10^5 $Pasm^{-2}$. Inserting this value into eq. 59 we find a prediction for the decay of the slope which is compared with the experimental result in figure 22. In spite of the crudeness of the approximations the agreement is quite satisfactory.

Wave reflections

Finally, the observed wave reflections in figures 9 and 10 can straight forward be explained from linear theory, leading to eq. 68. In figure 23a the jump is shown in the compliant "sinus" case. At the left the pressure jump is shown in the "sinus" and at the right the one in the "aorta". Due to the small length of the "sinus" region in comparison with the wave length a monotonic increase of pressure is found, which however converges quite well to the theory line. In case of a stiffer "sinus" region, see figure 23b, both theory and experiment show the large oscillations close to the valve and smaller ones in the "aorta".

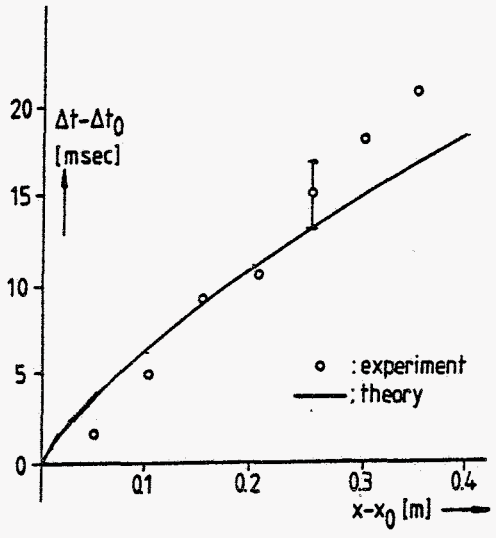

Fig. 22: The rise-time of the pressure jump as function of position compared with the (crude) visco-elastic model prediction.

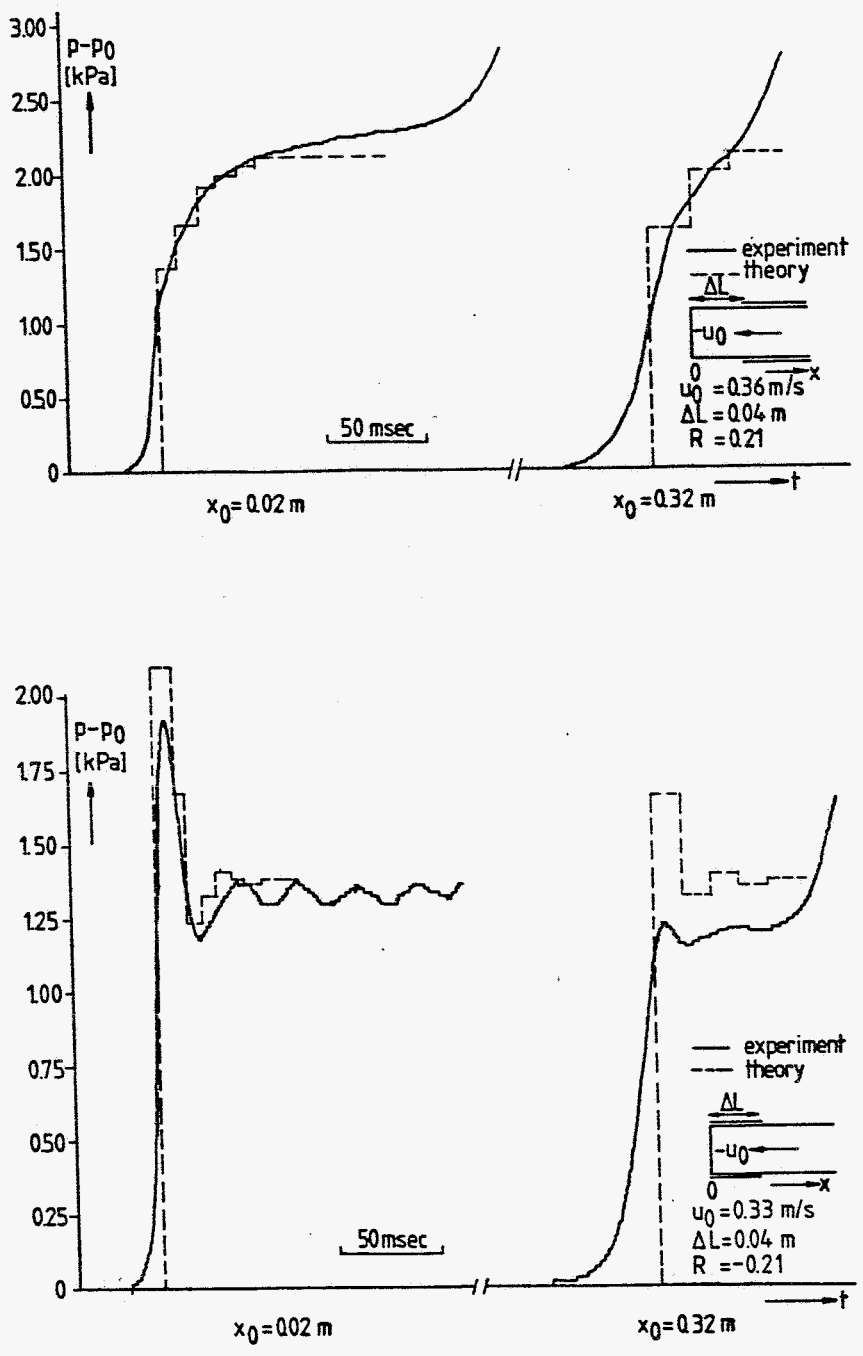

Fig. 23: The pressure jumps close to the valve and in the connecting tube in cases of a, b more compliant and c, d less compliant "sinus" section than the remaining tube.

Concluding discussion

In conclusion it is stated that the present model experiments reveal that wave phenomena in a long uniform tube can be determined accurately by means of the present experimental method and that they are partly well described by the one-dimensional laws of mass and momentum. The pressure height appeared to be affected by non-linearities and wall shear stress, and in the inhomogeneous case by the compliance of the sinus region. Our experiments also indicate that wall viscosity is the dominant factor in the gradual flattening of the wave form. This was also predicted from the theoretical analysis using an oversimplifying material model. The gradual pressure increase after the pressure jump is found to be caused by the influence of wall shear stress. For future research the next three shortcomings has to be raised. Firstly, a better material model has to be used, for example in the way Holenstein et al. (1984) did for arteries. Secondly, a better estimate of the initial wall shear stress has to be determined. Finally, coupling of the tensile experiments and diameter-pressure relationship is needful. Due to the relatively large pre-strain ($\sim$ 7%), linear theory predicts a compliance value which is about 60% lower than observed in the experiments. Hence an analysis of non-linear elastic deformation has to be performed, in which for example the latex is assumed to behave as a Mooney-Rivlin material (Ogden 1984). This all will be the subject of future research.

With regard to the medical implications of this study it is stated that the magnitude of the pressure rise just after valve closure is primarily determined by the back flow velocity. Hence it is worthwhile to develop a prosthetic leaflet valve which exhibits the natural gradual way of closure. Furthermore, the magnitude as well as the rise time of the pressure jump close to the valve are strongly determined by the compliance of the sinus region with regard to the aortic one. Therefore, it is important that in case of a prosthetic leaflet valve the sinus region remains its compliance and that it is not stiffened due to the operation procedure.

Acknowledgement

Appendix

Substition of eqs. 39 and 40 in eq. 36 yields after integration:

A1 $$\hat{v}^{(1)} - \hat{u}^{(1)} = \frac{1}{2}\int (1 + \hat{u}_v(\sigma))\, e^{-\xi_1/2}\, d\sigma$$

$$= \frac{1}{2}\, \hat{I}_v\, e^{-\xi_1/2}$$

A2 where: $$\hat{I}_v = \int (1 + \hat{u}_v(\sigma))\, d\sigma$$

The expression for $\hat{v}^{(1)}$ from A1 is substituted into eq. 33b

A3 $$2\,\frac{\partial \hat{u}^{(1)}}{\partial \xi_1} + \hat{u}^{(1)} = \frac{1}{4}\, \hat{I}_v\, e^{-\xi_1/2}$$

with solution:

A4 $$\hat{u}^{(1)} = \frac{1}{8}\, \hat{I}_v(\sigma)\, \xi_1\, e^{-\xi_1/2}$$

The expression for $v^{(1)}$ follows then from A1:

A5 $$\hat{v}^{(1)} = \frac{1}{2}\, \hat{I}_v\, (1 + \frac{1}{4}\, \xi_1) e^{-\xi_1/2}$$

References

Anliker M., Stettler J.C., Niederer P. and Holenstein R.: In: The arterial system, Springer-Verlag, 1978.

Bellhouse B.J. and Talbot L.: J. Fluid Mech. 35, 721-735, 1969.

Bergel D.H.: J. Physiol. 156, 445-457, 1961.

Bergel D.H.: J. Physiol. 156, 458-469, 1961.

Collins R., Flaud P., Geiger D., Kivity Y., Odou C.: Biomechanics Sofia, 1976.

Cowley S.J.: J. Fluid Mech. 116, 459-473, 1982.

Cox R.H.: Biophysical Journ. 8, 691-709, 1968.

Euler L. 1775: In: Opera Posthuma Mathematica et Physica anno 1844 Detecta 2, 814-823, 1862.

Fung Y.C.: In: Biomechanics, Its Foundations and Objectives, Prentice-Hall, 1972.

Fung Y.C.: Biodynamics (circulation), Springer-Verlag, 1984.

Holenstein R., Niederer P. and Anliker M.: J. Biomech. Engng. 102, 318-325, 1980.

Holenstein R., Nerem R.M. and Niederer P.: J. Biomech. Engng. 106, 115-122, 1984.

Kamm R.D. and Shapiro A.H.: J. Fluid Mech. 95, 1-78, 1979.

Kivity Y. and Collins R.: Archives of Mechanics 26, 921-931, 1974.

Kuiken G.D.C.: Ph.D.-thesis, Delft University of Technology, 1984.

Lambossy P.: Helv. Physiol. Acta 8, 209-227, 1950.

Lighthill M.J.: Mathematical Biofluiddynamics, Reg. Conf. Series in Appl. Mech., 1975.

Lighthill M.J.: Waves in fluids, Cambridge University Press, 1978.

Ling S.C. and Atabek H.B.: J. Fluid Mech. 55, 493-511, 1972.

Milnor W.R.: Hemodynamics, Williams and Wilkins, 1982.

Odou C., Dantan P., Flaud P. and Geiger D.: In: Quantitative Cardiovascular Studies, University Park Press, 1979.

Ogden R.W.: Non-linear elastic deformations, John Wiley, 1984.

Olson J.H. and Shapiro A.H.: J. Fluid Mech. 29, 513-538, 1967.

Pedley T.J.: The fluid mechanics of large blood vessels, Cambridge University Press, 1980.

Rudinger G.: J. Appl. Mech. 37, 34-37, 1970.

Sauren A.A.H.J., van Hout M.C., van Steenhoven A.A., Veldpaus F.E. and Janssen J.D.: J. Biomech. 16, 327-337, 1983.

Schlichting H.: Boundary layer theory, McGraw-Hill, 1979.

Shapiro A.H.: J. Biomech. Engng. 99, 126-147, 1977.

van Steenhoven A.A. and van Dongen M.E.H.: J. Fluid Mech. 90, 21-36, 1979.

van Steenhoven A.A., Verlaan C.W.J., Veenstra P.C. and Reneman R.S.: Am. J. Physiol. 240, H286-H292, 1981.

van Steenhoven A.A., Veenstra P.C. and Reneman R.S.: J. Biomech. 15, 941-950, 1982.

van Steenhoven A.A., van Duppen Th.J.A.G., Cauwenberg J.W.G. and van Renterghem R.J.: J. Biomech. 15, 841-848, 1982.

Weinbaum S. and Parker K.H.: J. Fluid Mech. 69, 729-752, 1975.

Wetterer E. and Kenner Th.: Grundlagen der Dynamik des Arterienpulses, Springer-Verlag, 1968.

Whitham G.B.: Linear and nonlinear waves, Wiley-Interscience, 1974.

Womersley J.R.: Technical Report WADC-TR-56-614, 1957.

Young T.: Phil. Trans. Roy. Soc. 98, 164-186, 1808.

Nawoord

De belangrijkste tekortkomingen van deze studie zijn:

- de verklaring van de uitdijing van het golffront op basis van de visceuze eigenschappen van de vaatwand is niet bevredigend, aangezien het gehanteerde materiaal model niet in overeenstemming is met het waargenomen nagenoeg constant zijn van de visceuze parameter over een groot reksnelheidsbereik, zie fig. 3/4;
- de verklaring van de afname van het golffront op basis van de visceuze eigenschappen van de vloeistof schiet duidelijk tekort;
- de koppeling tussen de materiaaleigenschappen van het latex (fig. 2-4) en de gemeten druk-diameter relatie (fig. 13/14) is niet uitgewerkt.

Met betrekking tot de voortgang van dit onderzoek stellen we ons dan ook het volgende voor:

- de visceuze eigenschappen van het materiaal te beschrijven met de gelineariseerde versie van de visco-elasticiteitsrelatie zoals o.a. gebruikt door Fung. Analoog aan de werkwijze ontwikkeld door Sauren (1982), worden de materiaalparameters K, θ_1 en θ_2 bepaald uit de relaxatiecurve van het proefstrookje. Op een gelijke wijze als aangegeven door Holenstein (1984) wordt vervolgens gepoogd de invloed van de daarmee corresponderende term in het rechterlid van vergelijking 47a uit te werken;
- ter analyse van de bijdrage van de vloeistofstroming aan de afname van de druksprong als functie van positie, wordt het experiment nogmaals uitgevoerd maar dan zodanig dat de druksprong stroomafwaarts gaat in plaats van stroomopwaarts. Ook zou de visceuze drukval voor klepsluiting nauwkeuriger gemeten dienen te worden. Daartoe ontbreekt ons vooralsnog de meetapparatuur.
- de voorspelling van de compliantie van de buis op basis van lineaire theorie:

$$C = \frac{2\pi R_0^3(1-\nu^2)}{h_0 E_0}$$

leidt, gebruikmakend van de beginhelling uit figuur 2, tot een onderschatting van de gemeten compliantie met zo'n 70%. De oorzaak hiervan moet waarschijnlijk gezocht worden in de eindige rek (7%) onder invloed van het initiële drukverschil over de buis (3 kPa). Een analyse op basis van niet-lineaire elastische deformatie waarbij het latex wordt voorgesteld als een Mooney-Rivlin materiaal (Ogden 1984) lijkt perspectief te bieden. Verdere uitwerking van het model en toetsing aan experimentele gegevens is de benodigde volgende stap.

Een belangrijk vraagpunt daarbij is evenwel waar het huidige verhaal is af te sluiten en een nieuw begint.